

# Dimerization induced mobility edges and multiple reentrant localization transitions in non-Hermitian quasicrystals

Wenqian Han<sup>1</sup> and Longwen Zhou<sup>1,\*</sup>

<sup>1</sup>*College of Physics and Optoelectronic Engineering,  
Ocean University of China, Qingdao 266100, China*

(Dated: 2022-02-18)

Non-Hermitian effects could create rich dynamical and topological phase structures. In this work, we show that the collaboration between lattice dimerization and non-Hermiticity could generally bring about mobility edges and multiple localization transitions in one-dimensional quasicrystals. Non-Hermitian extensions of the Aubry-André-Harper (AAH) model with staggered onsite potential and dimerized hopping amplitudes are introduced to demonstrate our results. Reentrant localization transitions due to the interplay between quasiperiodic gain/loss and lattice dimerization are found. Quantized winding numbers are further adopted as topological invariants to characterize transitions among phases with distinct spectrum and transport nature. Our study thus enriches the family of non-Hermitian quasicrystals by incorporating effects of lattice dimerization, and offering a convenient way to modulate localization transitions and mobility edges in non-Hermitian systems.

## I. INTRODUCTION

Non-Hermitian systems have attracted increasing attention over the past decade due to their abundant dynamical, topological and transport properties (see Refs. [1–6] for reviews). Theoretical studies have uncovered physics and phenomena that are unique to non-Hermitian settings, such as the exceptional points [7–9], non-Hermitian skin effects [10–13], anomalous localization transitions [14–17] and enlarged symmetry classifications of topological matter [18–22]. Experimental progress has also made it possible to observe novel nonunitary dynamics and non-Hermitian topological phases in a variety of platforms, ranging from cold atoms [23–25], photonics [26–29], acoustics [30–32], electrical circuits [33–35] to NV center in diamonds [36]. These developments further suggest potential applications of non-Hermitian effects in topological lasers [37–39] and high-performance sensors [40–43].

Recently, the interplay between non-Hermitian effects and spatial quasiperiodicity has been found to generate a rich class of matter called non-Hermitian quasicrystal (NHQC) [44–72]. In an NHQC, onsite gain and loss or nonreciprocal hoppings could induce  $\mathcal{PT}$ -breaking transitions of the spectrum from real to complex and localization transitions of eigenstates between extended and localized phases. Moreover, in certain situations, a critical phase could appear in between the extended and localized phases, which holds energy-dependent mobility edges separating delocalized and localized states [50, 51]. In a Hermitian quasicrystal, critical mobility edge phases could generally appear when the system possesses long-range hoppings [73–75] or dimerized lattice structures [76–78]. However, much less is known about generic ways of inducing and controlling mobility edges and localization transitions in non-Hermitian systems [64, 65].

In this work, we introduce a simple scheme to generate critical phases with mobility edges and create multiple reentrant localization transitions in NHQCs by adding experimentally implementable spatial dimerization to the onsite potential or hopping amplitudes. In Sec. II, we introduce general theoretical tools that can be used to unveil the spectral, localization, topological transitions and mobility edges in NHQCs. In Sec. III, we present models that will be considered in this work and discuss their common features. In Sec. IV, we reveal how staggered onsite potentials or dimerized hopping amplitudes could produce critical regions separating extended and localized phases in NHQCs, and how the change of dimerization effects could induce reentrant topological transitions among NHQC phases with distinct spectral and transport nature. In Sec. V, we summarize our results and discuss potential future studies.

## II. THEORY

We first outline the theoretical framework that will be adopted to investigate NHQCs in this work. We focus on one-dimensional (1D) systems with the following form of lattice Hamiltonian

$$H = \sum_{n \in \mathbb{Z}} (J_n^R |n\rangle \langle n+1| + J_n^L |n+1\rangle \langle n| + V_n |n\rangle \langle n|). \quad (1)$$

Here  $J_n^R$  ( $J_n^L$ ) describes the hopping amplitude from the  $(n+1)$ 's ( $n$ 's) to the  $n$ 's [ $(n+1)$ 's] site of the lattice.  $V_n$  is the amplitude of onsite potential. For a system with periodic boundary condition (PBC), we take the lattice site index  $n = 1, \dots, L$  and identify the basis  $|n\rangle = |n+L\rangle$ . The Hamiltonian  $H$  can be made non-Hermitian by either setting  $J_n^R \neq (J_n^L)^*$  (asymmetric hopping) or  $V_n \neq V_n^*$  (onsite gain and loss).  $H$  further describes a quasicrystal if we set  $J_n^{R,L}$  or  $V_n$  to a quasiperiodic function of  $n$ . In the lattice representation, the spectrum and states of  $H$  can be obtained by solving the eigenvalue

\* zhoulw13@u.nus.edu

equation  $H|\psi\rangle = E|\psi\rangle$ , yielding

$$J_n^R \psi_{n+1} + J_{n-1}^L \psi_{n-1} + V_n \psi_n = E \psi_n. \quad (2)$$

Here  $\psi_n$  represents the amplitude of wave function  $|\psi\rangle = \sum_n \psi_n |n\rangle$  on the  $n$ th lattice site. For a lattice of length  $L$ , there are  $L$  eigenenergies  $E = \{E_j | j = 1, \dots, L\}$ , whose values can in general be complex if  $H \neq H^\dagger$ .

In a system described by  $H$ , the presence of non-Hermiticity may induce three types of transitions [48]. On the spectral side, if  $H$  possesses the  $\mathcal{PT}$  or other types of symmetry that could make it pseudo-Hermitian, its spectrum can be real and the growth of its non-Hermitian parameters may induce a real-to-complex (e.g., the  $\mathcal{PT}$ -breaking) transition in the spectrum. Such a transition can be identified by looking at the maximum of the imaginary parts of  $E$  over all eigenstates, i.e.,

$$\max(\text{Im}E) = \max_{j \in \{1, \dots, L\}} (|\text{Im}E_j|). \quad (3)$$

It is clear that the value of  $\max(\text{Im}E)$  grows from zero to finite when the spectrum of  $H$  changes from real to complex, and vice versa. Besides, not all eigenstates may take complex energies after the spectrum transition. To reveal this fact, we introduce the density of states (DOSs) with complex eigenenergies

$$\rho = N(\text{Im}E \neq 0)/L, \quad (4)$$

where  $N(\text{Im}E \neq 0)$  denotes the number of states whose energies have finite imaginary parts. In the deep non-Hermitian region we would expect  $\rho \rightarrow 1$ .

An NHQC could generally possess a localized phase, an extended phase, and a critical phase in which localized and extended states coexist and are separated by a mobility edge [50, 51]. Different characteristics of these phases can be extracted from the level-spacing statistics and inverse/normalized participation ratios of the states. Assuming the eigenenergies  $\{E_j | j = 1, \dots, L\}$  are sorted by their real parts and denoting the real gap between the  $j$ th and  $(j-1)$ th energy levels as  $\varepsilon_j = \text{Re}E_j - \text{Re}E_{j-1}$ , we define adjacent gap ratios (AGRs) as  $g_j = \min(\varepsilon_j, \varepsilon_{j+1}) / \max(\varepsilon_j, \varepsilon_{j+1})$  for  $j = 2, \dots, L-1$ . Here  $\min(a, b)$  and  $\max(a, b)$  yield the minimum and maximum of  $a$  and  $b$ , respectively. The statistical feature of level-spacing is encoded in the average of AGRs over all states, which is defined as

$$\bar{g} = \frac{1}{L} \sum_j g_j. \quad (5)$$

In the limit  $L \rightarrow \infty$ , we have  $\bar{g} \rightarrow 0$  if all bulk states are extended, and  $\bar{g}$  approaches a constant in the localized phase [79–83]. In the critical phase, the value of  $\bar{g}$  is non-universal and changes between zero and its upper bound obtained for the localized phase. Meanwhile, if  $|\psi_j\rangle = \sum_{n=1}^L \psi_n^j |n\rangle$  is a normalized eigenstate of  $H$  with energy  $E_j$ , we define its inverse participation ra-

tio (IPR) and normalized participation ratio (NPR) as  $\text{IPR}_j = \sum_{n=1}^L |\psi_n^j|^4$  and  $\text{NPR}_j = (L \sum_{n=1}^L |\psi_n^j|^4)^{-1}$ . In the thermodynamic limit  $L \rightarrow \infty$ , we have  $\text{IPR}_j \rightarrow 0$  ( $\text{IPR}_j \rightarrow \xi_j^{-1}$ ) and  $\text{NPR}_j \rightarrow 1$  ( $\text{NPR}_j \rightarrow 0$ ) if  $|\psi_j\rangle$  is an extended (a localized) state, where the localization length  $\xi_j$  could be energy-dependent [84]. With the help of IPRs and NPRs, we can distinguish the three phases and capture the transitions among them from the following quantities:

$$\max(\text{IPR}) = \max_{j \in \{1, \dots, L\}} (\text{IPR}_j), \quad (6)$$

$$\min(\text{IPR}) = \min_{j \in \{1, \dots, L\}} (\text{IPR}_j), \quad (7)$$

$$\eta = \log_{10}(\langle \text{IPR} \rangle \langle \text{NPR} \rangle). \quad (8)$$

Here  $\langle \text{IPR} \rangle = \frac{1}{L} \sum_{j=1}^L \text{IPR}_j$  and  $\langle \text{NPR} \rangle = \frac{1}{L} \sum_{j=1}^L \text{NPR}_j$  denote the average of IPRs and NPRs over all states. When  $L \rightarrow \infty$ , we would have  $\max(\text{IPR}) \rightarrow 0$  if the system resides in an extended phase,  $\min(\text{IPR}) > 0$  if the system stays in a localized phase, and  $\eta$  to be finite if the system is in a critical phase with mobility edges [77]. The AGRs, IPRs and NPRs can thus be used to distinguish extended, localized and critical phases of an NHQC from complementary perspectives. Note in passing that in this work, our calculations are performed under the PBC. In this case, the non-Hermitian skin effect is absent and will not affect the spatial distribution of bulk states. Therefore, we compute the IPR and NPR for all bulk states using right eigenvectors, whereas using left eigenvectors will generate equivalent results concerning Eqs. (6)-(8).

When the energies of an NHQC possess imaginary parts, they may develop loop structures on the complex plane. Interestingly, the emergence of these complex energy loops was found to be related to the localization transitions in NHQCs. One can then introduce spectral winding numbers as topological order parameters to characterize phases with different transport nature and signify the transitions among them in an NHQC [47, 48]. The generic definition of such a winding number is

$$w_\ell = \lim_{L \rightarrow \infty} \int_0^{2\pi} \frac{d\theta}{2\pi i} \partial_\theta \ln \{ \det[H(\theta) - \mathcal{E}_\ell] \}. \quad (9)$$

Here  $\theta$  can be viewed as a flux penetrating through the ring formed by the system under PBC. The model Hamiltonian  $H$  in Eq. (1) can be changed to its  $\theta$ -dependent form  $H(\theta)$  by either setting  $J_n^{R(L)}$  to  $J_n^{R(L)} e^{+(-)i\theta/N}$  or adding a phase shift  $\theta/N$  to  $V_n$ , where  $N$  is the number of cells of the lattice. For the models considered in this work, the ways of introducing phase factor  $\theta$  to  $H$  are summarized in Table I.  $\mathcal{E}_\ell$  is a model-dependent base energy on the complex plane, and  $w_\ell$  counts the number of times the spectrum of  $H(\theta)$  winds around  $\mathcal{E}_\ell$  when  $\theta$  is swept over a period. If the system has no critical phases,

there is only one  $\mathcal{E}_\ell = \mathcal{E}_1$ , which can be chosen as the real part of energy of the first eigenstate of  $H$  whose IPR deviates from zero. The transition of the system from the extended to localized phases would then accompany the quantized jump of  $w_1$ . If the extended and localized phases of the system are further separated by a critical phase, another base energy  $\mathcal{E}_\ell = \mathcal{E}_2$  is needed, which can be chosen as the real part of energy of the last eigenstate of  $H$  whose IPR departures from zero. In this case, we expect  $w_1$  ( $w_2$ ) to take a quantized jump when the system goes from the extended (critical) phase to the critical (localized) phase [64]. Within a given phase, the winding number will be pinned to a quantized value and can thus be interpreted as a topological order parameter of the corresponding NHQC phase.

We are now ready to introduce explicit models with staggered onsite potentials or dimerized hopping amplitudes, and show how the interplay between lattice dimerization and non-Hermitian effects could create rich phase and transition patterns in NHQCs.

### III. MODEL

To uncover the impact of lattice dimerization on NHQCs, we start with the model introduced in Ref. [49], whose Hamiltonian takes the form  $H_0 = \sum_{n \in \mathbb{Z}} (J|n\rangle\langle n+1| + \text{H.c.} + V e^{i2\pi\alpha n}|n\rangle\langle n|)$ . Here  $J, V \in \mathbb{R}$  and  $\alpha = \frac{\sqrt{5}-1}{2}$ . As a non-Hermitian extension of the AAH model [85–87],  $H_0$  forms a minimal construction of an NHQC. It was proved that when  $|V| < |J|$ , the spectrum of  $H_0$  is real and all its eigenstates are extended. When  $|V| > |J|$ , the spectrum becomes complex and all eigenstates are localized. Therefore, the system described by  $H_0$  undergoes a  $\mathcal{PT}$ -breaking transition together with a localization transition at  $|V| = |J|$ , which can be topologically characterized by the quantized jump of a spectral winding number [69]. Note that no critical phases and mobility edges are found in  $H_0$ , and all states undergo the same localization transition when  $|V|$  switches from below to above  $|J|$ , with the common Lyapunov exponent  $\lambda = \ln|V/J|$  [49].

Another NHQC model that will be employed has the Hamiltonian  $H_1 = \sum_{n \in \mathbb{Z}} (J|n\rangle\langle n+1| + \text{H.c.} + V \cos(2\pi\alpha n + i\gamma)|n\rangle\langle n|)$ , where  $i\gamma$  introduces an imaginary phase shift in the superlattice potential. It was found that when  $\gamma = \gamma_c = \ln|2J/V|$ , the states of  $H_1$  could undergo a transition from an extended phase with real spectrum ( $|\gamma| < |\gamma_c|$ ) to a localized phase with complex spectrum ( $|\gamma| > |\gamma_c|$ ) [48]. This transition is further accompanied by the quantized jump of a spectral winding number  $w$  for zero to  $-1$  [48]. However, there are also no signatures of critical mobility edge phases in the system described by  $H_1$ , and all eigenstates experience the same spectral and localization transitions at  $\gamma = \gamma_c$ .

In this work, we use dimerized versions of  $H_0$  and  $H_1$  to showcase our main results. We consider three different extensions, which are denoted by M1–M3. Their Hamil-

tonians share the form of Eq. (1) with components listed in Table I. In M1–M3, the strength of hopping dimerization and staggered onsite potential are separately controlled by the parameters  $\Lambda$  and  $\Delta$ . For the calculations presented below, we choose  $J = 1$  as the unit of energy, let  $\alpha = (\sqrt{5}-1)/2$  be the inverse golden ratio and assuming PBC throughout. It will be shown that the dimerization effects could generically induce critical phases with mobility edges, and furthermore trigger alternated and reentrant localization transitions in NHQCs.

## IV. RESULTS

We now investigate the spectral, localization and topological transitions in M1–M3 with the tools introduced in Sec. II. We first consider the effect of lattice dimerization in onsite potential (M1) and hopping amplitudes (M2) in Subsecs. IV A and IV B. Both of these two types of dimerization are found to induce critical phases with mobility edges and multiple localization transitions in the presence of non-Hermitian quasiperiodic potential. In Subsec. IV C, we unveil intriguing patterns of reentrant localization transitions in M3, which are due to the interplay between onsite dimerization and dissipation.

### A. M1: Effect of staggered onsite potential

Referring to Table I, the M1 corresponds to a non-Hermitian variant of the AAH model plus a staggered onsite potential. Following Eq. (2), the Hamiltonian of M1 reads  $H = \sum_n (|n\rangle\langle n+1| + \text{H.c.} + V_n|n\rangle\langle n|)$  and its eigenvalue equation takes the form  $\psi_{n+1} + \psi_{n-1} + V_n\psi_n = E\psi_n$ , where  $V_n = V e^{i2\pi\alpha n} + (-1)^n\Delta$  and we have set  $J = 1$  as the unit of energy. Since  $V_n = V_{-n}^*$ , M1 possesses the  $\mathcal{PT}$ -symmetry, implying that its spectrum could be real in certain parameter regions. Under the PBC, the spectrum of M1 for a typical set of onsite dimerization  $\Delta$  are shown in Figs. 1(a)–(c). We observe that with the increase of  $\Delta$ , the spectrum could change from purely real [Fig. 1(a)] to a mixture of real and complex energies [Fig. 1(b)], and finally be purely complex [Fig. 1(c)]. Therefore, the presence of staggered onsite potential in M1 could not only induce a  $\mathcal{PT}$ -breaking transition of the spectrum, but also create an intermediate region with coexisting real and complex eigenenergies, which is absent when  $\Delta = 0$ . Compared with the single transition of  $H_0$  as mentioned in Sec. III, the introduction of a staggered onsite potential could clearly enrich the spectral patterns of NHQCs. In Fig. 1(d), we further show the maximum of the imaginary part of spectrum versus the quasiperiodic non-Hermitian potential  $V$  and onsite dimerization  $\Delta$ . For  $V \in (0, 1)$ , we find a  $\mathcal{PT}$ -breaking transition of the spectrum from real ( $\max|\text{Im}E| = 0$ ) to complex ( $\max|\text{Im}E| > 0$ ) with the increase of either  $V$  or  $\Delta$ . For  $V > 1$ , the system enters a phase with only complex energies, and the change

Model index	Hopping amplitudes $J_n^{L,R}$	Onsite potential $V_n$	Onsite potential with phase shift $V_n(\theta)$
M1	$J$	$V e^{i2\pi\alpha n} + (-1)^n \Delta$	$V e^{i(2\pi\alpha n + \theta/N)} + (-1)^n \Delta$
M2	$J + (-1)^n \Lambda$	$V e^{i2\pi\alpha n}$	$V e^{i(2\pi\alpha n + \theta/N)}$
M3	$J$	$V \cos(2\pi\alpha n + i\gamma) + (-1)^n \Delta$	$V \cos(2\pi\alpha n + i\gamma + \theta/N) + (-1)^n \Delta$

TABLE I. NHQCs with staggered onsite potential or dimerized hopping amplitudes. The system parameters  $J, V, \Delta, \Lambda, \gamma \in \mathbb{R}$ , and the lattice site index  $n \in \mathbb{Z}$ .  $\alpha$  is irrational and set as  $\frac{\sqrt{5}-1}{2}$  throughout this work.  $N = L/2$  is the number of dimerized cells in the lattice of length  $L$ . In the calculation of winding numbers, the Hamiltonians  $H$  of M1–M3 are replaced by  $H(\theta)$  via changing their  $V_n$  in the third column to the corresponding  $V_n(\theta)$  in the last column.

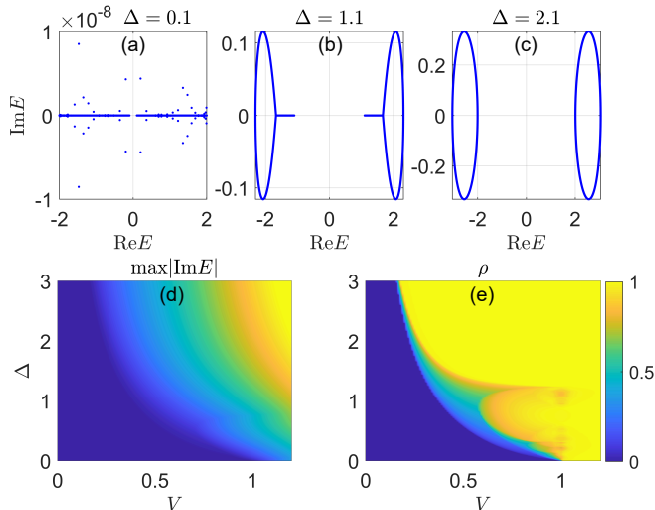


FIG. 1. Spectral properties of M1 under the PBC. The length of lattice is  $L = 2584$  for all panels. (a)–(c) show the spectrum of M1 at  $V = 0.5$  with the increase of staggered onsite potential  $\Delta$ . (d) exhibits the maximum of imaginary parts of energies versus  $V$  and  $\Delta$ . (e) denotes the DOSs with nonvanishing imaginary parts of energies. (d) and (e) share the same color bar.

of  $\Delta$  would not create further spectral transitions. In Fig. 1(e), we present the DOSs [Eq. (4)] with complex eigenenergies  $\rho$  versus  $V$  and  $\Delta$ , which show three qualitatively distinct regions. At the bottom left corner (in blue), we have  $\rho = 0$  and all eigenstates of  $H$  have real energies. At the top right corner (in yellow), we have  $\rho = 1$  and the eigenenergies of all states are complex. In between the former two regions, we find  $0 < \rho < 1$ , implying the eigenstates therein form a mixture of real and complex energies. Notably, this intermediate region is absent without the dimerization in onsite potential. Furthermore, as will be discussed shortly, the states in these three regions possess distinct localization and topological features.

To decode the localization transitions in M1, we study its averaged AGRs [Eq. (5)], IPRs [Eqs. (6)–(7)] and the measure  $\eta$  [Eq. (8)] characterizing the presence of a critical phase with mobility edge. In Fig. 2(a), we find three different regions in  $\bar{g}$  versus  $V$  and  $\Delta$ , which have one-to-one correspondences with the three regions of spectrum in Fig. 1(e). Therefore, we expect M1 to show an ex-

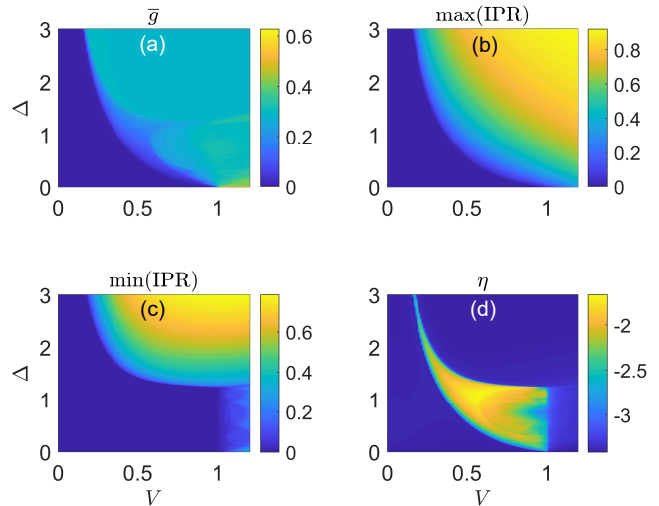


FIG. 2. State properties of M1, computed with the length of lattice  $L = 2584$  under the PBC. (a) shows the averaged AGRs [Eq. (5)]. (b) and (c) show the maximum [Eq. (6)] and minimum [Eq. (7)] of IPRs over all states at different system parameters  $(V, \Delta)$ . (d) presents the function  $\eta$  [Eq. (8)], which is finite only in the critical phase with mobility edge.

tended phase ( $\bar{g} = 0$ ) with real spectrum, a localized phase ( $\bar{g} \simeq 0.3$ ) with purely complex spectrum, and a critical phase  $0 < \bar{g} \lesssim 0.3$  in which eigenstates with real and complex energies coexist and are separated by a mobility edge. These inferences are further confirmed by the numerical results of  $\max(\text{IPR})$  ( $= 0$  only if all eigenstates are extended),  $\min(\text{IPR})$  ( $> 0$  only if all eigenstates are localized) and  $\eta$  (finite only if localized and extended states coexist), as presented in Figs. 2(b)–2(d). Therefore, the presence of onsite dimerization and its interplay with the non-Hermitian quasiperiodicity could indeed yield a critical phase with mobility edge, and induce multiple transitions in NHQCs.

The transitions among extended, critical, and localized phases in M1 can be further attached with quantized jumps of topological invariants. According to Eq. (9), we construct a pair of winding numbers  $w_1$  and  $w_2$  to characterize the transitions from extended to critical and from critical to localized phases in M1, respectively. Note that for M1–M2, the phase shift in Eq. (9) is introduced by setting  $V e^{i2\pi\alpha n} \rightarrow V e^{i(2\pi\alpha n + 2\theta/L)}$  in  $V_n$ , where  $L/2$  corresponds to the number of dimerized cells. By calculating

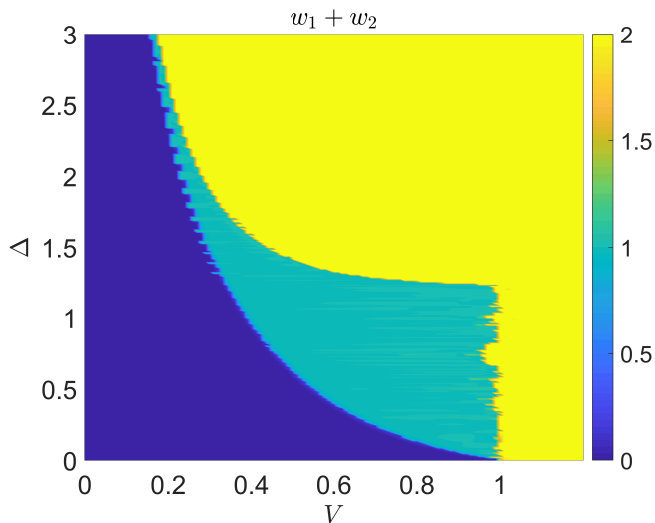


FIG. 3. Topological phase diagram of M1 under the PBC. The regions in blue, green and yellow correspond to the extended, critical and localized NHQC phases with winding numbers  $(w_1, w_2) = (0, 0)$ ,  $(1, 0)$  and  $(1, 1)$ , respectively. The length of lattice is set as  $L = 610$  in the calculation.

$(w_1, w_2)$ , we obtain the topological phase diagram of the system, as presented in Fig. 3. We find a region (in blue) with winding numbers  $(w_1, w_2) = (0, 0)$ , which is in coincidence with the extended phase with real spectrum, a second region (in green) with  $(w_1, w_2) = (1, 0)$ , which is consistent with the critical phase with partially real spectrum, and a third region (in yellow) with  $(w_1, w_2) = (1, 1)$  coinciding with the localized phase with purely complex spectrum in Figs. 1 and 2. These results clearly demonstrate that the spectral winding numbers  $(w_1, w_2)$  could be employed as topological order parameters to distinguish the three NHQC phases of M1 and characterize the transitions among them. Put together, the existence of staggered onsite potential could indeed induce  $\mathcal{PT}$ -breaking, multiple localization and topological transitions, and also yield a critical phase with mobility edge. It can therefore be used as a flexible knob to tune and even create intriguing phases and transitions in NHQCs.

In Sec. IV B, we show that multiple localization transitions and mobility edges could also be induced in NHQCs by adding dimerization to the hopping amplitudes.

### B. M2: Effect of dimerized hopping amplitudes

We now investigate a non-Hermitian AAH model with dimerized hopping amplitudes, whose Hamiltonian takes the form  $H = \sum_n (J_n |n\rangle\langle n+1| + \text{H.c.} + V_n |n\rangle\langle n|)$ , with  $J_n = 1 + (-1)^n \Lambda$  and  $V_n = V e^{i2\pi\alpha n}$  as given by M2 in Table I. The resulting eigenvalue equation is  $J_n \psi_{n+1} + J_{n-1} \psi_{n-1} + V_n \psi_n = E \psi_n$ , and the uniform part of hopping is set to  $J = 1$ . In experiments, the dimerized hopping amplitudes can be realized in various physical platforms. For example, in cold atom systems, it can be

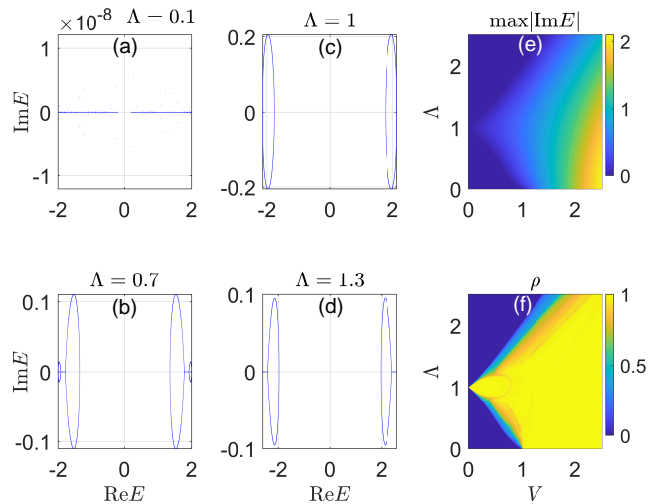


FIG. 4. Spectral properties of M2 under the PBC. The length of lattice is  $L = 2584$  for all panels. (a)–(d) show the spectrum at  $V = 0.5$  with the increase of staggered hopping amplitude  $\Lambda$ . (e) presents the maximum of imaginary parts of energy versus  $V$  and  $\Lambda$ . (f) shows the DOSs with nonvanishing imaginary parts of energy.

engineered by superimposing two standing optical waves of wavelengths  $\lambda$  and  $2\lambda$  to generate a lattice potential of the form  $U \sin^2(2\pi x/\lambda + \phi/2) + U' \sin^2(4\pi x/\lambda + \pi/2)$ , where  $x$  denotes the position and  $\phi$  represents a controllable phase between the two standing wave fields of strengths  $U$  and  $U'$  [88–90]. Since  $J_n = J_{-n}^*$  and  $V_n = V_{-n}^*$ , M2 also obeys the  $\mathcal{PT}$ -symmetry, which means that its spectrum can be real in some parameter domains. Note that a different non-Hermitian extension of M2 was considered in Ref. [64], and dimerization-induced intermediate phases with mobility edges were also observed.

When  $V \in (0, 1)$ , M2 undergoes four spectral transitions with the increase of hopping dimerization  $\Lambda$ . Typical spectra of the system before and after these transitions are shown in Figs. 4(a)–4(d). With the increase of  $\Lambda$ , M2 first goes through a  $\mathcal{PT}$ -breaking transition from a real spectrum [Fig. 4(a)] to a mixed spectrum with both real and complex eigenvalues [Fig. 4(b)]. At a larger  $\Lambda$ , states with real energies vanish and the spectral becomes purely complex [Fig. 4(c)]. However, with the further increase of  $\Lambda$ , real eigenvalues in the spectrum re-emerge and the system goes back to a phase with coexisting real and complex energies, as shown in Fig. 4(d). When  $\Lambda$  becomes even larger, M2 could again enter the phase with real spectrum and the  $\mathcal{PT}$ -symmetry is recovered, which corresponds to the region with  $\max|\text{Im}E| = 0$  at the top left corner of Fig. 4(e). The DOSs with complex energies shown in Fig. 4(f) further confirms the observed alternating transitions among real, mixed and complex spectrum regions. The physical mechanism behind these reentrant spectral transitions may be understood as follows. With the increase of  $\Lambda$ , the averaged hopping amplitudes

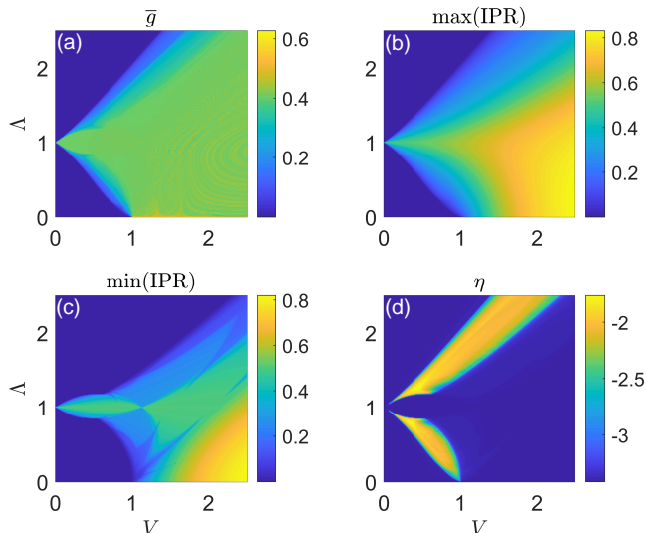


FIG. 5. State properties of M2, computed with the length of lattice  $L = 2584$  under the PBC. (a) shows the average of AGRs over all states [Eq. (5)]. (b) and (c) show the maximum [Eq. (6)] and minimum [Eq. (7)] of IPRs at different system parameters ( $V, \Lambda$ ). (d) shows the quantity  $\eta$  [Eq. (8)], whose value is finite only in critical phases with mobility edges.

among lattice sites, which may be expressed as a function  $f(J - \Lambda, J + \Lambda)$  does not change monotonically with  $\Lambda$ . Since the spectrum transitions in M2 are originated from the competition between hopping and onsite energy scales, the non-monotonic behavior of  $f(J - \Lambda, J + \Lambda)$  in  $\Lambda$  implies the non-monotonic process of spectral transitions.

Similar to the cases encountered in M1, the spectral transitions in M2 are also accompanied by state transitions among extended, critical, and localized phases. This is demonstrated by the results presented in Fig. 5, which describe the averaged AGRs [Fig. 5(a)], IPRs [Fig. 5(b)–(c)] and the measure of critical phase with mobility edges  $\eta$  [Fig. 5(d)]. From the minimum and maximum of IPRs, we can clearly see two distinct phase boundaries at  $\max(\text{IPR}) = 0 \rightarrow > 0$  and  $\min(\text{IPR}) = 0 \rightarrow > 0$ , respectively, across which the system changes from the extended to critical and from the critical to localized phases. These phase boundaries coincide with the parameters at which the DOSs with complex energies change from  $0 \rightarrow \rho \in (0, 1)$  and from  $\rho \in (0, 1) \rightarrow 1$  in Fig. 4(f). The critical phases in which extended and localized states coexist are highlighted by the regions with finite values of  $\eta$  in Fig. 5(d). These two sets of states are separated in energy by mobility edges. Notably, there are two such critical regions separated by a localized phase for  $V \in (0, 1)$ . These phases are originated from the interplay between dimerized hoppings and non-Hermitian quasiperiodic potential. Therefore, with the increase of  $\Lambda$ , the system could undergo multiple and reentrant transitions among extended, critical, and localized NHQC phases. Each transition is accompanied by a

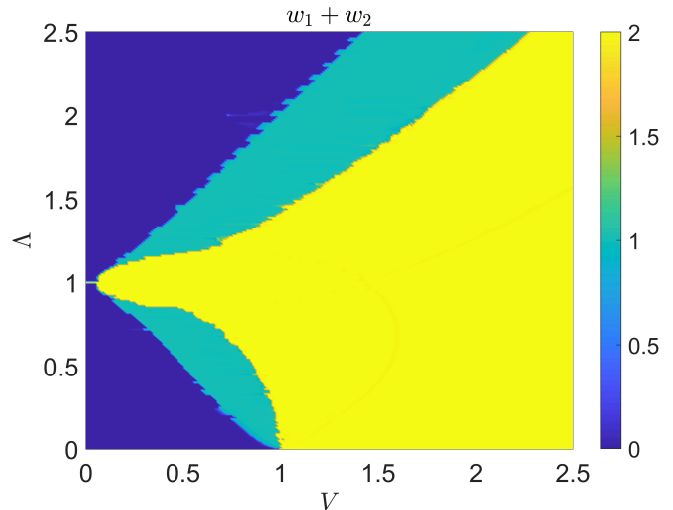


FIG. 6. Topological phase diagram of M2 under the PBC. Regions in blue, green and yellow correspond to the extended, critical and localized NHQC phases with spectral winding numbers  $(w_1, w_2) = (0, 0)$ ,  $(1, 0)$ , and  $(1, 1)$ , respectively. The length of lattice is chosen to be  $L = 610$ .

drastic change in the structure of spectrum.

With the help of Eq. (9), we obtain the spectral winding numbers  $(w_1, w_2)$  of M2, leading to the topological phase diagram presented in Fig. 6. Together with the results shown in Figs. 4 and 5, we see that there are indeed three distinct topological NHQC phases in M2. The extended phase (with real spectrum) and localized phase (with complex spectrum) possess winding numbers  $(w_1, w_2) = (0, 0)$  and  $(w_1, w_2) = (1, 1)$ , whereas the critical phase (with mobility edge) has  $(w_1, w_2) = (1, 0)$ . When  $V \in (0, 1)$ , we could encounter four topological transitions with the increase of hopping dimerization  $\Lambda$ . At a fixed  $\Lambda$  ( $\neq 0, 1$ ), M2 will first change from the extended to critical phase, and finally enter the localized phase with the increase of non-Hermitian potential  $V$ . The critical phases with  $(w_1, w_2) = (1, 0)$  separating the extended and localized ones are present only if  $\Delta \neq 0$  in M2. Put together, we conclude that both dimerized onsite and hopping modulations could induce critical regions with mobility edges in NHQCs and control transitions among phases with distinct spectral, localization and topological nature.

### C. M3: Multiple reentrant localization transitions

In the last example, we consider the case in which the non-Hermiticity is introduced by an imaginary phase shift in the AAH model with a staggered onsite potential, leading to the M3 in Table I. The Hamiltonian of M3 takes the form  $H = \sum_n (|n\rangle\langle n+1| + \text{H.c.} + V_n |n\rangle\langle n|)$  with  $V_n = V \cos(2\pi\alpha n + i\gamma) + (-1)^n \Delta$ . The eigenvalue equation reads  $\psi_{n+1} + \psi_{n-1} + V_n \psi_n = E \psi_n$ . Since  $V_n = V_n^*$ ,  $H$  here also possesses the  $\mathcal{PT}$ -symmetry and its spec-

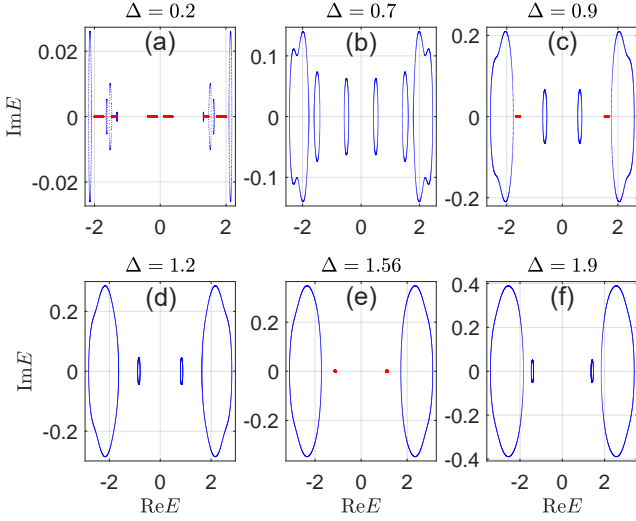


FIG. 7. Typical spectra of M3, obtained for a lattice of length  $L = 2584$  under the PBC. States with real (complex) eigenenergies are denoted by red stars (blue dots). The values of dimerization parameter  $\Delta$  are listed in the captions of (a)–(f). Other system parameters are set as  $(J, V, \gamma) = (1, 1, 0.5)$ .

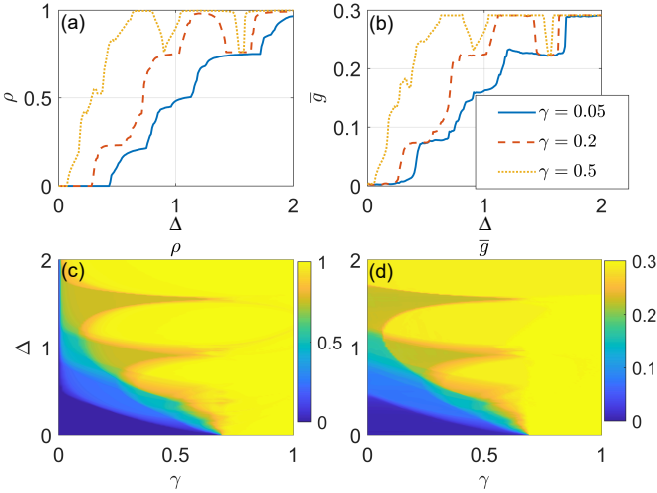


FIG. 8. Spectral properties and AGRs of M3, obtained for a lattice of length  $L = 2584$  and under the PBC. Other system parameters are  $(J, V) = (1, 1)$ . The solid, dashed and dotted lines in (a) and (b) show the DOSs [Eq. (4)] and AGRs [Eq. (5)] versus the onsite dimerization  $\Delta$  for different  $\gamma$ . In (c) and (d), the DOSs and AGRs versus both  $\gamma$  and  $\Delta$  show consistent patterns for  $\gamma \neq 0$ .

trum could be real. With the increase of the staggering strength  $\Delta$ , spectral and localization transitions would also occur in M3 as demonstrated below. Most notably, triggered by onsite dimerization, the system is found to be able to roam alternately between localized and critical mobility edge phases in a non-monotonic way.

In Fig. 7, we present selected spectra of M3 under different strengths of lattice dimerization. We observe that with a finite amount of imaginary phase shift  $i\gamma$ , the num-

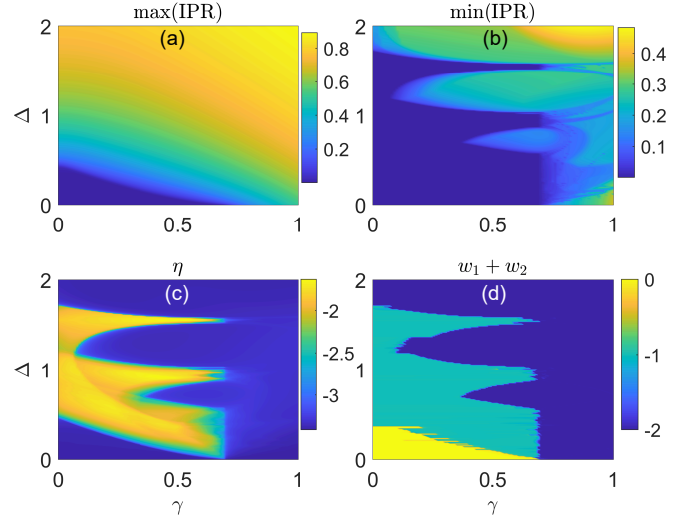


FIG. 9. State properties and winding numbers of M3 obtained under the PBC. System parameters are  $(J, V) = (1, 1)$ . (a)–(c) show the maximum [Eq. (6)], minimum [Eq. (7)] of IPRs and  $\eta$  [Eq. (8)] at different system parameters  $(\gamma, \Delta)$ , computed with a lattice size  $L = 2584$ . (d) shows the topological phase diagram, in which yellow, green and blue regions correspond to the extended, critical and localized NHQC phases with spectral winding numbers  $(w_1, w_2) = (0, 0)$ ,  $(-1, 0)$ , and  $(-1, -1)$ , respectively, computed with a lattice size  $L = 610$ .

ber of real eigenvalues in the spectrum could change with  $\Delta$  in a highly non-monotonic manner. Specifically, the real eigenvalues in the spectrum vanish when  $\Delta$  changes from 0.2 to 0.7, but re-emerge when  $\Delta$  goes from 0.7 to 0.9. This process could repeat until  $\Delta$  is large enough and all states end in taking complex energies. These rich and non-monotonic behaviors of spectrum are closely related to the reentrant localization and topological transitions of M3.

In Fig. 8, we present the DOSs with nonzero imaginary parts of energy  $\rho$  and AGRs  $\bar{g}$  versus the phase shift  $\gamma$  and onsite dimerization  $\Delta$ . Close to the Hermitian limit ( $\gamma \simeq 0$ ), we find a transition of the system from real ( $\rho = 0$ ) to complex ( $\rho > 0$ ) spectrum with the increase of  $\Delta$ , which goes together with the change of  $\bar{g}$  from zero to a finite value  $0 < \bar{g} \lesssim 0.3$ . The further increase of  $\Delta$  causes a second transition, after which  $\rho$  and  $\bar{g}$  approach 1 and 0.3. Surprisingly, when  $\gamma$  is away from zero but still smaller than the critical value  $\gamma_c = \ln |2J/V|$ , we find  $\rho$  and  $\bar{g}$  to show reentrant behaviors between the phases with  $\rho \in (0, 1)$ ,  $\bar{g} \in (0, 0.3)$ , and  $\rho = 1$ ,  $\bar{g} \simeq 0.3$ , which are clearly demonstrated by the dashed and dotted lines shown in Figs. 8(a)–8(b). These reentrant transitions, which are absent if  $\Delta = 0$  in M3, are expected to be consistent with the alternation of the system between localized and critical phases through a series of topological localization transitions, as confirmed by the results presented in Figs. 9(a)–9(d). For example, near  $\gamma = 0.5$ , the system is found to follow a sequence of transitions from extended  $\rightarrow$  critical  $\rightarrow$  localized  $\rightarrow$

critical  $\rightarrow$  localized  $\rightarrow$  critical, and finally ends in a localized phase with the increase of onsite dimerization  $\Delta$ . This transition sequence is further accompanied by the changes of winding numbers following  $(w_1, w_2) = (0, 0) \rightarrow (-1, 0) \rightarrow (-1, -1) \rightarrow (-1, 0) \rightarrow (-1, -1) \rightarrow (-1, 0)$ , and finally arrives at  $(w_1, w_2) = (-1, -1)$ . Note that for M3, the phase shift in Eq. (9) is introduced by setting  $i\gamma \rightarrow i\gamma + 2\theta/L$  in  $V_n$ . Therefore, we conclude that the lattice dimerization could not only produce critical phases with mobility edges, but also induce multiple and reentrant topological localization transitions in NHQCs. Notably, the reentrant transitions found here are different from those observed in Hermitian quasicrystals [77], as in our case these transitions are only found at finite amounts of imaginary phase shift  $i\gamma$ , implying that they are unique phenomena originated from the interplay between non-Hermiticity and spatial dimerization. Moreover, the alternating jumps of topological order parameters endow richer structures to the reentrant transitions in NHQCs compared with their Hermitian counterparts [76–78], providing us with more insights to non-Hermitian disordered systems from a topological perspective.

## V. SUMMARY

In this work, we found lattice dimerization induced critical phases with mobility edges and multiple reentrant localization transitions in NHQCs. These findings were explicitly demonstrated in non-Hermitian extensions of the AAH model with staggered onsite potentials or dimerized hopping amplitudes. Especially, the interplay between dimerization and non-Hermitian effects works as a flexible knob to control the phase transitions and critical properties of NHQCs. Moreover, topolog-

ical order parameters were employed to precisely distinguish extended, critical, localized phases of NHQCs and capture the transitions among them. Put together, our results unveil the richness of NHQC phases in the presence of lattice dimerization, uncover the chance of generating reentrant localization transitions in NHQCs, and suggest a way to manipulate the transport nature of NHQCs by tuning dimerization effects. In Refs. [76–78], multiple and/or reentrant localization transitions are found in quasicrystals with lattice dimerization or during the process in which one type of quasicrystal changes to another. In all the cases, the systems under consideration are described by Hermitian Hamiltonians. Compared with these former studies, our work uncovers the role played by the collaboration of non-Hermitian effects and lattice dimerization in generating reentrant localization and topological phase transitions that are unique to non-Hermitian settings. In future work, it would be interesting to consider lattice dimerization in different types of NHQC models, such as those with nonreciprocal hoppings, and explore more exotic phases of dimerized NHQCs in the presence of many-body interactions and time-periodic drives. The possible interplay between lattice dimerization and the recently found pseudo mobility edges [91] due to non-Hermitian skin effects also deserve more thorough explorations.

## ACKNOWLEDGMENTS

L.Z. is supported by the National Natural Science Foundation of China (Grant No. 11905211), the Young Talents Project at Ocean University of China (Grant No. 861801013196), and the Applied Research Project of Postdoctoral Fellows in Qingdao (Grant No. 861905040009).

- 
- [1] E. J. Bergholtz, J. C. Budich, and F. K. Kunst, Exceptional topology of non-Hermitian systems, *Rev. Mod. Phys.* **93**, 015005 (2021).
  - [2] Y. Ashida, Z. Gong, and M. Ueda, Non-Hermitian physics, *Adv. Phys.* **69**, 249-435 (2020).
  - [3] R. El-Ganainy, K. G. Makris, M. Khajavikhan, Z. H. Musslimani, S. Rotter, and D. N. Christodoulides, Non-Hermitian physics and PT symmetry, *Nat. Phys.* **14**, 11-19 (2018).
  - [4] A. Ghatak and T. Das, New topological invariants in non-Hermitian systems, *J. Phys.: Condens. Matter* **31**, 263001 (2019).
  - [5] V. M. Martinez Alvarez, J. E. Barrios Vargas, M. Berdakin, and L. E. F. Foa Torres, Topological states of non-Hermitian systems, *Eur. Phys. J. Spec. Top.* **227**, 1295 (2018).
  - [6] C. Coulais, R. Fleury, and J. van Wezel, Topology and broken Hermiticity, *Nat. Phys.* **17**, 9-13 (2021).
  - [7] M. V. Berry, Physics of Nonhermitian Degeneracies, *Czech. J. Phys.* **54**, 1039 (2004).
  - [8] W. D. Heiss, The physics of exceptional points, *J. Phys. A: Math. Theor.* **45**, 444016 (2012).
  - [9] M.-A. Miri and A. Alù, Exceptional points in optics and photonics, *Science* **363**, eaar7709 (2019).
  - [10] S. Yao and Z. Wang, Edge States and Topological Invariants of Non-Hermitian Systems, *Phys. Rev. Lett.* **121**, 086803 (2018).
  - [11] F. K. Kunst, E. Edvardsson, J. C. Budich, and E. J. Bergholtz, Biorthogonal Bulk-Boundary Correspondence in Non-Hermitian Systems, *Phys. Rev. Lett.* **121**, 026808 (2018).
  - [12] V. M. Martinez Alvarez, J. E. Barrios Vargas, and L. E. F. Foa Torres, Non-Hermitian robust edge states in one dimension: anomalous localization and eigenspace condensation at exceptional points, *Phys. Rev. B* **97**, 121401(R) (2018).
  - [13] C. H. Lee and R. Thomale, Anatomy of skin modes and topology in non-Hermitian systems, *Phys. Rev. B* **99**, 201103(R) (2019).



- [14] N. Hatano and D. R. Nelson, Localization Transitions in Non-Hermitian Quantum Mechanics, *Phys. Rev. Lett.* **77**, 570 (1996).
- [15] J. Feinberg and A. Zee, Non-Hermitian localization and delocalization, *Phys. Rev. E* **59**, 6433 (1999).
- [16] J. Feinberg and A. Zee, Spectral curves of non-hermitian hamiltonians, *Nucl. Phys. B* **552**, 599-623 (1999).
- [17] N. Hatano and J. Feinberg, Chebyshev-polynomial expansion of the localization length of Hermitian and non-Hermitian random chains, *Phys. Rev. E* **94**, 063305 (2016).
- [18] Z. Gong, Y. Ashida, K. Kawabata, K. Takasan, S. Higashikawa, and M. Ueda, Topological Phases of Non-Hermitian Systems, *Phys. Rev. X* **8**, 031079 (2018).
- [19] K. Kawabata, K. Shiozaki, M. Ueda and M. Sato, Symmetry and Topology in Non-Hermitian Physics, *Phys. Rev. X* **9**, 041015 (2019).
- [20] H. Zhou and J. Y. Lee, Periodic table for topological bands with non-Hermitian symmetries, *Phys. Rev. B* **99**, 235112 (2019).
- [21] C. C. Wojcik, X. Sun, T. Bzdušek, and S. Fan, Homotopy characterization of non-Hermitian Hamiltonians, *Phys. Rev. B* **101**, 205417 (2020).
- [22] K. Shiozaki and S. Ono, Symmetry indicator in non-Hermitian systems, *Phys. Rev. B* **104**, 035424 (2021).
- [23] W. Gou, T. Chen, D. Xie, T. Xiao, T.-S. Deng, B. Gadway, W. Yi, and B. Yan, Tunable Nonreciprocal Quantum Transport through a Dissipative Aharonov-Bohm Ring in Ultracold Atoms, *Phys. Rev. Lett.* **124**, 070402 (2020).
- [24] J. Li, A. K. Harter, J. Liu, L. d. Melo, Y. N. Joglekar, and L. Luo, Observation of parity-time symmetry breaking transitions in a dissipative Floquet system of ultracold atoms, *Nat. Commun.* **10**, 855 (2019).
- [25] Y. Xu, S.-T. Wang, and L.-M. Duan, Weyl Exceptional Rings in a Three-Dimensional Dissipative Cold Atomic Gas, *Phys. Rev. Lett.* **118**, 045701 (2017).
- [26] J. M. Zeuner, M. C. Rechtsman, Y. Plotnik, Y. Lumer, S. Nolte, M. S. Rudner, M. Segev, and A. Szameit, Observation of a Topological Transition in the Bulk of a Non-Hermitian System, *Phys. Rev. Lett.* **115**, 040402 (2015).
- [27] S. Weimann, M. Kremer, Y. Plotnik, Y. Lumer, S. Nolte, K. G. Makris, M. Segev, M. C. Rechtsman, and A. Szameit, Topologically protected bound states in photonic parity-time-symmetric crystals, *Nat. Mater.* **16**, 433-438 (2017).
- [28] K. Wang, X. Qiu, L. Xiao, X. Zhan, Z. Bian, B. C. Sanders, W. Yi, and P. Xue, Observation of emergent momentum-time skyrmions in parity-time-symmetric non-unitary quench dynamics, *Nat. Commun.* **10**, 2293 (2019).
- [29] L. Xiao, T. Deng, K. Wang, G. Zhu, Z. Wang, W. Yi, and P. Xue, Non-Hermitian bulk-boundary correspondence in quantum dynamics, *Nat. Phys.* **16**, 761-766 (2020).
- [30] W. Zhu, X. Fang, D. Li, Y. Sun, Y. Li, Y. Jing, and H. Chen, Simultaneous Observation of a Topological Edge State and Exceptional Point in an Open and Non-Hermitian Acoustic System, *Phys. Rev. Lett.* **121**, 124501 (2018).
- [31] C. Shen, J. Li, X. Peng, and S. A. Cummer, Synthetic exceptional points and unidirectional zero reflection in non-Hermitian acoustic systems, *Phys. Rev. Mater.* **2**, 125203 (2018).
- [32] H. Gao, H. Xue, Q. Wang, Z. Gu, T. Liu, J. Zhu, and B. Zhang, Observation of topological edge states induced solely by non-Hermiticity in an acoustic crystal, *Phys. Rev. B* **101**, 180303(R) (2020).
- [33] T. Hofmann, T. Helbig, F. Schindler, N. Salgo, M. Brzezinska, M. Greiter, T. Kiessling, D. Wolf, A. Vollhardt, A. Kabaši, C. H. Lee, A. Bilušić, R. Thomale, and T. Neupert, Reciprocal skin effect and its realization in a topological circuit, *Phys. Rev. Res.* **2**, 023265 (2020).
- [34] T. Helbig, T. Hofmann, S. Imhof, M. Abdelghany, T. Kiessling, L. W. Molenkamp, C. H. Lee, A. Szameit, M. Greiter, and R. Thomale, Generalized bulk-boundary correspondence in non-Hermitian topoelectrical circuits, *Nat. Phys.* **16**, 747-750 (2020).
- [35] S. Liu, S. Ma, C. Yang, L. Zhang, W. Gao, Y. J. Xiang, T. J. Cui, and S. Zhang, Gain- and Loss-Induced Topological Insulating Phase in a Non-Hermitian Electrical Circuit, *Phys. Rev. Appl.* **13**, 014047 (2020).
- [36] Y. Wu, W. Liu, J. Geng, X. Song, X. Ye, C.-K. Duan, X. Rong, and J. Du, Observation of parity-time symmetry breaking in a single-spin system, *Science* **364**, 878-880 (2019).
- [37] G. Harari, M. A. Bandres, Y. Lumer, M. C. Rechtsman, Y. D. Chong, M. Khajavikhan, D. N. Christodoulides, and M. Segev, Topological insulator laser: Theory. *Science* **359**, 4003 (2018).
- [38] M. A. Bandres, S. Wittek, G. Harari, M. Parto, J. Ren, M. Segev, D. N. Christodoulides, and M. Khajavikhan, Topological insulator laser: Experiments. *Science* **359**, 4005 (2018).
- [39] Y. V. Kartashov and D. V. Skryabin, Two-Dimensional Topological Polariton Laser, *Phys. Rev. Lett.* **122**, 083902 (2019).
- [40] J. Wiersig, Enhancing the Sensitivity of Frequency and Energy Splitting Detection by Using Exceptional Points: Application to Microcavity Sensors for Single-Particle Detection, *Phys. Rev. Lett.* **112**, 203901 (2014).
- [41] H.-K. Lau and A. A. Clerk, Fundamental limits and non-reciprocal approaches in non-Hermitian quantum sensing, *Nat. Commun.* **9**, 4320 (2018).
- [42] H. Hodaei, A. U. Hassan, S. Wittek, H. Garcia-Gracia, R. El-Ganainy, D. N. Christodoulides, and M. Khajavikhan, Enhanced sensitivity at higher-order exceptional points, *Nature* **548**, 187-191 (2017).
- [43] W. Chen, S. K. Özdemir, G. Zhao, J. Wiersig, and L. Yang, Exceptional points enhance sensing in an optical microcavity, *Nature* **548**, 192-196 (2017).
- [44] P. Sarnak, Spectral Behavior of Quasi Periodic Potentials, *Commun. Math. Phys.* **84**, 377-401 (1982).
- [45] A. Jazaeri and I. I. Satija, Localization transition in incommensurate non-Hermitian systems, *Phys. Rev. E* **63**, 036222 (2001).
- [46] Q. Zeng, S. Chen, and R. Lü, Anderson localization in the non-Hermitian Aubry-André-Harper model with physical gain and loss, *Phys. Rev. A* **95**, 062118 (2017).
- [47] H. Jiang, L. Lang, C. Yang, S. Zhu, and S. Chen, Interplay of non-Hermitian skin effects and Anderson localization in nonreciprocal quasiperiodic lattices, *Phys. Rev. B* **100**, 054301 (2019).
- [48] S. Longhi, Topological Phase Transition in non-Hermitian Quasicrystals, *Phys. Rev. Lett.* **122**, 237601 (2019).
- [49] S. Longhi, Metal-insulator phase transition in a non-Hermitian Aubry-André-Harper model, *Phys. Rev. B*

- 100**, 125157 (2019).
- [50] T. Liu, H. Guo, Y. Pu, and S. Longhi, Generalized Aubry-André self-duality and mobility edges in non-Hermitian quasiperiodic lattices, *Phys. Rev. B* **102**, 024205 (2020).
- [51] Y. Liu, X.-P. Jiang, J. Cao, and S. Chen, Non-Hermitian mobility edges in one-dimensional quasicrystals with parity-time symmetry, *Phys. Rev. B* **101**, 174205 (2020).
- [52] Q. Zeng, Y. Yang, and R. Lü, Topological phases in one-dimensional nonreciprocal superlattices, *Phys. Rev. B* **101**, 125418 (2020).
- [53] Q. Zeng, Y. Yang, and Y. Xu, Topological phases in non-Hermitian Aubry-André-Harper models, *Phys. Rev. B* **101**, 020201(R) (2020).
- [54] L. Zhai, S. Yin, and G. Huang, Many-body localization in a non-Hermitian quasiperiodic system, *Phys. Rev. B* **102**, 064206 (2020).
- [55] Q. Zeng and Y. Xu, Winding numbers and generalized mobility edges in non-Hermitian systems, *Phys. Rev. Res.* **2**, 033052 (2020).
- [56] S. Longhi, Phase transitions in a non-Hermitian Aubry-André-Harper model, *Phys. Rev. B* **103**, 054203 (2021).
- [57] Y. Liu, Y. Wang, Z. Zheng, and S. Chen, Exact non-Hermitian mobility edges in one-dimensional quasicrystal lattice with exponentially decaying hopping and its dual lattice, *Phys. Rev. B* **103**, 134208 (2021).
- [58] Y. Liu, Y. Wang, X. Liu, Q. Zhou, and S. Chen, Exact mobility edges, PT-symmetry breaking, and skin effect in one-dimensional non-Hermitian quasicrystals, *Phys. Rev. B* **103**, 014203 (2021).
- [59] Z. Xu and S. Chen, Dynamical evolution in a one-dimensional incommensurate lattice with PT symmetry, *Phys. Rev. A* **103**, 043325 (2021).
- [60] X. Cai, Boundary-dependent self-dualities, winding numbers, and asymmetrical localization in non-Hermitian aperiodic one-dimensional models, *Phys. Rev. B* **103**, 014201 (2021).
- [61] L. Tang, G. Zhang, L. Zhang, and D. Zhang, Localization and topological transitions in non-Hermitian quasiperiodic lattices, *Phys. Rev. A* **103**, 033325 (2021).
- [62] T. Liu, S. Cheng, H. Guo, and X. Gao, Fate of Majorana zero modes, exact location of critical states, and unconventional real-complex transition in non-Hermitian quasiperiodic lattices, *Phys. Rev. B* **103**, 104203 (2021).
- [63] L. Zhai, G. Huang, and S. Yin, Cascade of the delocalization transition in a non-Hermitian interpolating Aubry-André-Fibonacci chain, *Phys. Rev. B* **104**, 014202 (2021).
- [64] L. Zhou and W. Han, Non-Hermitian quasicrystal in dimerized lattices, *Chin. Phys. B* **30**, 100308 (2021).
- [65] Z.-H. Wang, F. Xu, L. Li, D. Xu, and B. Wang, Unconventional real-complex spectral transition and Majorana zero modes in nonreciprocal quasicrystals, *Phys. Rev. B* **104**, 174501 (2021).
- [66] Y. Liu, Q. Zhou, and S. Chen, Localization transition, spectrum structure, and winding numbers for one-dimensional non-Hermitian quasicrystals, *Phys. Rev. B* **104**, 024201 (2021).
- [67] X. Cai, Localization and topological phase transitions in non-Hermitian Aubry-André-Harper models with  $p$ -wave pairing, *Phys. Rev. B* **103**, 214202 (2021).
- [68] S. Longhi, Non-Hermitian Maryland model, *Phys. Rev. B* **103**, 224206 (2021).
- [69] L. Zhou, Floquet engineering of topological localization transitions and mobility edges in one-dimensional non-Hermitian quasicrystals, *Phys. Rev. Research* **3**, 033184 (2021).
- [70] A. P. Acharya, A. Chakrabarty, and D. K. Sahu, Localization, PT-Symmetry Breaking and Topological Transitions in non-Hermitian Quasicrystals, *Phys. Rev. B* **105**, 014202 (2022).
- [71] L. Zhou and J. Gu, Topological delocalization transitions and mobility edges in the nonreciprocal Maryland model, *J. Phys.: Condens. Matter* **34**, 115402 (2022).
- [72] X. Xia, K. Huang, S. Wang, and X. Li, Exact mobility edges in the non-Hermitian  $t_1 - t_2$  model: Theory and possible experimental realizations, *Phys. Rev. B* **105**, 014207 (2022).
- [73] R. B. Diener, G. A. Georgakis, J. Zhong, M. Raizen, and Q. Niu, Transition between extended and localized states in a one dimensional incommensurate optical lattice, *Phys. Rev. A* **64**, 033416 (2001).
- [74] D. J. Boers, B. Goedeke, D. Hinrichs, and M. Holthaus, Mobility edges in bichromatic optical lattices, *Phys. Rev. A* **75**, 063404 (2007).
- [75] X. Li, X. Li, and S. Das Sarma, Mobility edges in one dimensional bichromatic incommensurate potentials, *Phys. Rev. B* **96**, 085119 (2017).
- [76] V. Goblort, A. Štrkalj, N. Pernet, J. L. Lado, C. Dorow, A. Lemaître, L. Le Gratiet, A. Harouri, I. Sagnes, S. Ravets, A. Amo, J. Bloch, and O. Zilberberg, Emergence of criticality through a cascade of delocalization transitions in quasiperiodic chains, *Nat. Phys.* **16**, 832 (2020).
- [77] S. Roy, T. Mishra, B. Tanatar, and S. Basu, Reentrant Localization Transition in a Quasiperiodic Chain, *Phys. Rev. Lett.* **126**, 106803 (2021).
- [78] A. Padhan, M. K. Giri, S. Mondal and T. Mishra, Emergence of multiple localization transitions in a one-dimensional quasiperiodic lattice, arXiv:2109.09621.
- [79] I. Y. Goldsheid and B. A. Khoruzhenko, Distribution of Eigenvalues in Non-Hermitian Anderson Models, *Phys. Rev. Lett.* **80**, 2897 (1998).
- [80] L. G. Molinari, Non-Hermitian spectra and Anderson localization, *J. Phys. A: Math. Theor.* **42**, 265204 (2009).
- [81] H. Markum, R. Pullirsch, and T. Wettig, Non-Hermitian Random Matrix Theory and Lattice QCD with Chemical Potential, *Phys. Rev. Lett.* **83**, 484 (1999).
- [82] J. T. Chalker and B. Mehlh, Eigenvector Statistics in Non-Hermitian Random Matrix Ensembles, *Phys. Rev. Lett.* **81**, 3367 (1998).
- [83] R. Hamazaki, K. Kawabata, N. Kura, and M. Ueda, Universality classes of non-Hermitian random matrices, *Phys. Rev. Res.* **2**, 023286 (2020).
- [84] S. M. Girvin and K. Yang, *Modern Condensed Matter Physics* (Cambridge University Press, New York, 2019).
- [85] S. Aubry and G. André, Analyticity breaking and Anderson localization in incommensurate lattices, *Ann. Israel Phys. Soc.* **3**, 133 (1980).
- [86] P. G. Harper, Single band motion of conduction electrons in a uniform magnetic field, *Proc. Phys. Soc. London A* **68**, 874 (1955).
- [87] J. B. Sokoloff, Unusual band structure, wave function and electrical conductance in crystals with incommensurate periodic potentials, *Phys. Rep.* **126**, 189 (1985).
- [88] M. Atala, M. Aidelsburger, J. T. Barreiro, D. Abanin, T. Kitagawa, E. Demler, and I. Bloch, Direct measurement of the Zak phase in topological Bloch bands *Nat. Phys.* **9**, 795-800 (2013).

- [89] S. Nakajima, T. Tomita, S. Taie, T. Ichinose, H. Ozawa, L. Wang, M. Troyer, and Y. Takahashi, Topological Thouless pumping of ultracold fermions, *Nat. Phys.* **12**, 296-300 (2016).
- [90] M. Lohse, C. Schweizer, O. Zilberberg, M. Aidelsburger, and I. Bloch, A Thouless quantum pump with ultracold bosonic atoms in an optical superlattice, *Nat. Phys.* **12**, 350-354 (2016).
- [91] S. Mu, L. Zhou, L. Li, and J. Gong, Non-Hermitian pseudo mobility edge in a coupled chain system, arXiv:2111.11914.